From Field to Sky: Measurement and Modeling of Transgenic Switchgrass Pollen Dispersal in the Atmosphere

Manu Nimmala[a,*], Hope A. Gruszewski[b], Regina Hanlon[b], Landon Bilyeu[b], Tyler Newton[e], Jessica Stockdale[e], Reginald J. Millwood[e], Charles N. Stewart[e], Craig Powers[b], Shane D. Ross[c], Hosein Foroutan[d], and David G. Schmale III[b]

[a]Virginia Tech, Mechanical Engineering, Blacksburg, Virginia 24061, USA
[b]Virginia Tech, School of Plant and Environmental Sciences, Virginia 24061, USA
[c]Virginia Tech, Aerospace and Ocean Engineering, Blacksburg, Virginia 24061, USA
[d]Virginia Tech, Civil and Environmental Engineering, Blacksburg, Virginia 24061, USA
[e]University of Tennessee, Department of Plant Sciences, Knoxville, Tennessee 37996, USA
[*]nimmala@vt.edu

ABSTRACT

Accurate tracking and measurement of pollen dispersal in the atmosphere is essential for monitoring aeroallergens and assessing cross-pollination risks, particularly in the case of genetically engineered (GE) crops. We conducted a series of unique release-recapture field studies with GE switchgrass in Oliver Springs, TN. Two hundred transgenic switchgrass plants (*Panicum virgatum L.* 'Performer') were planted at the center of a clear-cut field, with one block of 100 plants expressing orange fluorescent protein (OFP) under a maize ubiquitin promoter (PvUBI1) and another block of 100 plants expressing OFP driven by a maize pollen-specific promoter (Zm13). Pollen was sampled from the atmosphere using fixed (ground-based) and mobile (drone-based) sampling devices at different distances from the source field, with Lagrangian Stochastic dispersal simulations run for sampling periods using high-resolution wind measurements. The pollen emission rate was estimated by combining simulated and measured pollen concentrations, and strong diurnal trends were observed. Diurnal emission rate trends were positively correlated with wind speed, temperature, and vapor pressure deficit, while negatively correlated with relative humidity. In low-wind meandering conditions, incorporating changing wind direction into the dispersal modeling improved pollen emission rate estimation and model-measurement comparisons. This study assesses the effectiveness of high and low volume pollen samplers in relation to source strength up to 1 km from the source, enhancing understanding of pollen measurement techniques. Additionally, it is a proof-of-concept for drone-based pollen sampling and GMO pollen tracking using fluorescence. Results from our experiments have significant implications for cross-pollination risk assessment, prediction, and management of airborne allergens.
Keywords: switchgrass, transgenic, pollen dispersal, bioaerosol, drone sampling, pollen transport, fluorescence

1 Introduction

Accurate tracking and measurement of pollen dispersal in the atmosphere is important for assessing cross-pollination risks (Aylor et al., 2003; Nimmala et al., 2024), particularly in the case of genetically-engineered (GE) crops. Wind-dispersed pollen is the primary method of gene flow in many grasses, including switchgrass (*Panicum virgatum*), an important bioenergy crop (Sofiev and Bergmann, 2012). It is a perennial, warm-season C4 bunchgrass found across most of eastern North America—from northern Mexico to southern Canada. Originally adopted as a forage crop, it is now a leading candidate for large-scale lignocellulosic biofuel feedstock in the U.S. and beyond (Parrish and Fike, 2005). There is increasing concern that the rapid growth and development of switchgrass as a biofuel could result in gene flow from GE switchgrass fields to nontransgenic fields (including wild populations), leading to both financial and ecological damage (Kwit and Stewart, 2012; Millwood et al., 2017; Ahrens et al., 2011; Ecker et al., 2015; Stockdale and Millwood, 2023). These changes could be compounded by the effects of climate change, where rising temperatures result in altered native switchgrass territory (Ahrens et al., 2014). Therefore, there is an urgent need for field experiments and modeling efforts to characterize the dispersal of airborne switchgrass pollen in relation to meteorological factors for regulation and risk management purposes.

There are limited experimental and modeling studies on switchgrass gene flow (Kwit and Stewart, 2012); these model pollen dispersal with and without wind breaks (Auer et al., 2016), experimentally quantify the dispersal and cross-pollination of transgenic switchgrass (Millwood et al., 2017), and model transport in low and high-wind conditions (Ecker et al., 2013). In

2011, Millwood and colleagues conducted the first regulated transgenic switchgrass field experiments in the U.S. (Millwood et al., 2017). A 3-year field experiment was performed in Oliver Springs, Tennessee, U.S.A. where 100 clonal switchgrass 'Alamo' plants transgenic for an orange-fluorescent protein (OFP) were used as the pollen source (whole plants, including pollen, were orange-fluorescent). To assess pollen movement, pollen traps were placed at 10 m intervals from the pollen-source plot in the four cardinal directions extending up 100 m from the field. Results showed that pollen-mediated gene flow is likely to occur over distances of at least 100 m (Millwood et al., 2017). This study provided important baseline data useful to determine isolation distances and other management practices, should transgenic switchgrass be grown commercially in relevant environments. Since switchgrass is an obligate outcrossing perennial grass, there are concerns about gene flow and the need for bioconfinement, especially for pollen (Kausch et al., 2010; Kwit and Stewart, 2012; Stockdale and Millwood, 2023). Moreover, since North America is the geographic center of switchgrass diversity, a better understanding of pollen movement in this species is needed (Kwit and Stewart, 2012).

The spread of pollen through the atmosphere involves processes of liberation, drift, and deposition (Aylor et al., 2003; Isard and Gage, 2001). Knowledge of these processes can help growers and producers make informed management decisions regarding pollen transport in seed production fields and neighboring farms (Isard and Gage, 2001). Although atmospheric transport models can predict pollen movement, they often fail to incorporate actual measurements of pollen concentrations and viability. Various unmanned aircraft systems (UASs or drones) have previously been used to detect and monitor pollen movement over long distances in the lower atmosphere. Gottwald and Tedders pioneered the collection of pollen with UASs (Gottwald and Tedders, 1985). They modified a remote-controlled biplane platform with two rotating drum samplers to collect pollen and plant pathogen spores over pecan and peach orchards. Their study demonstrated the significant potential for regional-scale transport of pollen and plant pathogens among orchards. Two decades later, Aylor and colleagues (Aylor et al., 2006) combined ground-based sampling devices with UASs to collect pollen within and above a cornfield. Over the past decade, Schmale and colleagues have integrated autonomous systems into UASs, enabling teams of vehicles to coordinate flight missions and perform complex atmospheric sampling tasks (Schmale III et al., 2008; Techy et al., 2010).

The allergen-management community needs a fast and reliable sensor network to measure airborne pollen concentrations to enable timely and accurate allergen reporting (Buters et al., 2018, 2024; Suanno et al., 2021; Tummon et al., 2021). Current allergen information reports only broad species group concentrations, typically at a daily resolution at best (Buters et al., 2018; Tummon et al., 2021). Future airborne pollen forecasts can be enhanced by integrating known pollen emissions with large-scale atmospheric models. Understanding diurnal pollen release patterns could aid in allergen treatment and improve emission source data for potential forecast models (Buters et al., 2018). To our knowledge, most airborne pollen field studies and corresponding allergen reports rely on Hirst-type samplers (Plaza et al., 2022). These sampling devices are constrained by a relatively low sampling rate of approximately 10 L/min (Adamov et al., 2024; Plaza et al., 2022), necessitating either high airborne pollen concentrations or extended sampling durations to accurately characterize pollen levels. The latter constraint contributes to the coarse temporal resolution of daily allergen pollen reporting.

We hypothesized that (1) wind-dispersed pollen from switchgrass could be tracked and quantified using orange fluorescent protein (OFP) expression, (2) a Lagrangian Stochastic (LS) dispersal model could estimate pollen source strength in the field, and (3) an array of novel samplers could serve as viable alternatives to standard Hirst-type samplers. To test these hypotheses, we conducted a series of unique release-recapture field studies using GE switchgrass in Oliver Springs, TN. Two hundred plants from five transgenic lines of switchgrass (*Panicum virgatum* L. 'Performer') were planted at the center of a clear-cut field. One block consisted of 100 plants expressing OFP under the control of a maize ubiquitin promoter (PvUBI1), while the other block contained 100 plants expressing OFP driven by a maize pollen-specific promoter (Zm13). Pollen from the atmosphere surrounding these blocks of transgenic switchgrass was collected using a series of fixed (ground-based) and mobile (drone-based) sampling devices at various distances from the field center. The efficacy of these various samplers was evaluated within 25 m of the source and up to 1 km from the source. LS dispersal simulations were conducted for pollen sampling periods using high-resolution wind measurements collected near the field. Pollen emission rates were estimated by combining simulated concentrations with field concentration measurements. By integrating high-resolution measurements and simulations, our study evaluates the performance of emerging sampling technologies and highlights their implications for biosecurity, allergen tracking, and ecological modeling.

2 Methodology

2.1 Field Site and Pollen Source

2.1.1 Field site

To assess the transport of wind-dispersed pollen from transgenic switchgrass plants, a two-year field study was conducted under USDA APHIS BRS release permits (21-094-103r and 124-86SS5F1). The experiments were carried out at the Tennessee Agricultural Experiment Station, near the University of Tennessee's Forest Resources Research and Education Center at the Cumberland Forest Unit in Oliver Springs, TN (36.0483147, -84.4811417).

The field site was selected for its large open area (∼1.5 ha), which provided sufficient space for switchgrass cultivation and pollen sampling while being surrounded by heavily forested borders. The borders acted as a natural barrier, limiting cross-contamination with both wild and cultivated switchgrass. The field plot measured 45' × 30', enclosed within a protective 50' × 65' fenced perimeter, as shown in Figure 1A. The outer fence was locked to prevent animal intrusion.

The field location was intentionally chosen in a remote, concealed area beyond a secured access point, ensuring restricted visibility and access. It was situated on recently cleared forest land, with felled trees surrounding a rough glade area.

2.1.2 Transgenic line generation, analysis, and selection

Transgenic switchgrass plants expressing OFP were created by genetically engineering embryogenic callus derived from switchgrass seeds obtained from Ernst Conservation Seeds, Inc. (Meadville, Pennsylvania, USA). This was achieved through Agrobacterium-mediated transformation (*Agrobacterium tumefaciens* strain EHA105) as detailed in Li and Qu (2011), using one of two binary plasmid constructs.

The first plasmid, pANIC10A-OFP (Mann et al., 2012), contained the hygromycin phosphotransferase (hph) selectable marker gene under the control of the switchgrass ubiquitin 2 (PvUbi2) promoter as well as an orange fluorescent protein (OFP) gene pporRFP under the control of the switchgrass ubiquitin promoter (PvUBI1). This promoter drives the expression of OFP in leaves, stems, and pollen.

The second plasmid, PSYBIN1a-Zm13-pporRFP, also contained the OFP gene pporRFP under the control of a maize pollen-specific promoter (Zm13). This promoter drives the expression of OFP in the pollen. This construct also contained a second OFP gene mOrangeER under the control of the cauliflower mosaic virus (CaMV) 35S promoter which enable the expression of this OFP in callus and green tissues. In addition, the plasmid also contained the hygromycin phosphotransferase (hph) selectable marker gene under the control of the PvUBI2 promoter. Several transgenic OFP-expressing shoots were recovered from hygromycin selection media (100 mg/L), and once rooted, plants were grown an environmental-controlled growth room (16/8 h day/night and 24/22°C day/night).

To confirm the presence of the OFP gene in the transgenic plants, PCR-screening was performed using primers (forward primer: GCAAAGTGGGGTCAAAGATG; reverse primer: CACCTTCAAGCCCTTCTTTG) designed to amplify a 556 bp fragment of the pporRFP gene. PCR-confirmed transgenic plants were moved to a greenhouse and grown (16/8 h day/night and 28/22°C day/night) until flowering. To identify transgenic events expressing OFP in pollen, visual analysis of OFP fluorescence was conducted on pollen grains from each event using epifluorescent microscopy as described by Rice et al. (2013). Transgenic lines in which all pollen grains exhibited OFP expression were propagated in the greenhouse and subsequently used in field experiments.

2.1.3 Planting

The planted area, less than 0.1 ha, consisted of 20 rows with 20 switchgrass plants per row, totaling 400 transgenic switchgrass plants arranged in a randomized design. These plants were hand-transplanted in the field at 76.2 cm intervals on three different dates. On July 20, 2021, 100 pANIC10A-OFP switchgrass plants from five transgenic events (20 clonal replicates per event) were transplanted. On August 26, 2021, another 100 PSYBIN1a-Zm13-pporRFP plants from five transgenic events (20 clonal replicates per event) were transplanted. Lastly, on June 20, 2022, an additional 200 pANIC10A-OFP switchgrass plants from ten transgenic events (20 clonal replicates per event) were transplanted in the field site. These last 200 plants were not mature enough to produce pollen during the field experiments. Figure 1B illustrates the locations of these plants and their ages in weeks during the August 2-3, 2022 field experiment. This experimental design was structured to monitor and analyze the dispersal from transgenic pollen over time and distance.

2.2 Sampling Methods

Four types of volumetric particle samplers, shown in Figure 3, were used to capture GE switchgrass pollen and estimate the concentration of airborne pollen at various times and distances from the source field. Each sampler had different sampling rates and sensing capabilities. To optimize equipment placement, wind forecasts and local conditions were assessed before the first sampling period. The samplers were strategically positioned based on prevailing and predicted wind directions, ensuring placement downwind of the expected pollen dispersal path. Figure 2 illustrates the placement of samplers around the field on each sampling day. The samplers were placed on reddish-orange circular drone landing pads to mark their locations and enhance visibility in overhead footage, as shown in Figure 1A for the August 2-3, 2022 field campaign.

2.2.1 Ground-based high-volume samplers (ED)

In anticipation of low pollen emission rates, several high-volume filter-based samplers (Science First #15000, Yulee, FL) (Science First, 2007) were deployed during the campaign (Figure 3A). Originally designed for educational use in schools, these samplers are referred to as "ED" samplers throughout the manuscript.

The barrel-shaped ED samplers draw air through a filter surface at an initial flow rate of 600 L/min (Science First, 2007). Cellulose filters with a pore size of 11 μm and a diameter of 125 mm were used to collect airborne pollen and other atmospheric

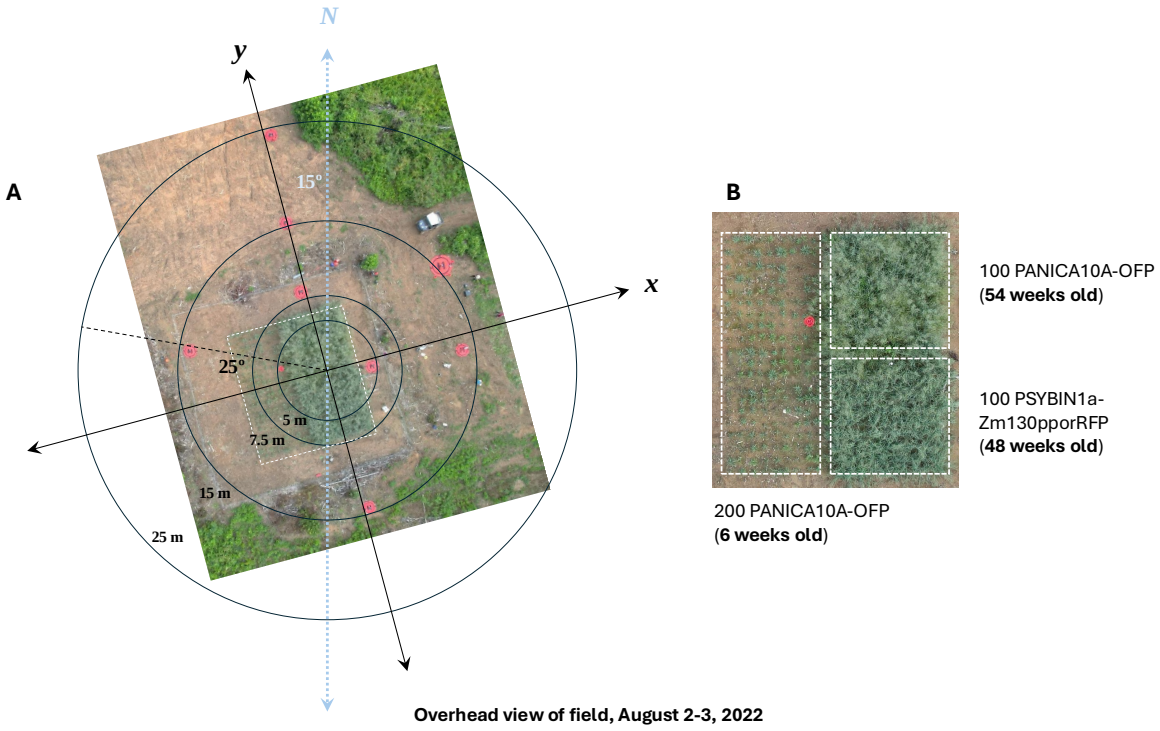

Figure 1. Top-down drone image of the field during field experiments conducted on August 2-3, 2022. (A) The field of GE switchgrass is outlined by a white dotted square and enclosed by a perimeter fence, as required by the APHIS BRS permits. Reddish-orange circular pads mark the locations of pollen sampling devices, positioned at increasing distances from the center of the source field. (B) A close-up view of the 45' × 30' field of GE Switchgrass, showing the locations of both strains of OFP-expressing switchgrass plants. Labels indicate the plant positions and ages during the August 2-3, 2022, field campaign.

particles at 0.432 m above ground level. The ED samplers' volumetric sampling rate is 1000 times that of the IMP and DRN samplers, and 35 times that of the FRM sampler. This significant increase in sampling capacity allowed for improved detection of airborne pollen, particularly in cases of low pollen emission rates.

2.2.2 Ground-based medium-volume sampler (FRM)

A single near-Federal Reference Method (FRM) sampler (ARA Instruments, Eugene, Oregon) was deployed during the field experiments, shown in Figure 3B. This battery-operated device samples air at a flow rate of 16.7 L/min. The unit is equipped with a filter sampler (PM_{10} filters were used in this study), meteorological sensors, and a particle counter. Additional details about this instrument are available on ARA's website (ARA Instruments, 2016).

2.2.3 Ground-based low-volume samplers (Impingers or IMP)

To evaluate the effectiveness of impinger-type samplers, three custom-designed impinger packages were deployed during the field campaign (Figure 3C) . These sampling packages are referred to as "IMP" throughout the manuscript.

The IMPs were constructed from high-density polyethylene, following the design specifications outlined in Powers et al. (2018). The 3D-printing (.stl) files for the impinger units are publicly available online (Powers, C., 2018). These files were modified to accommodate a 15 mL polypropylene conical collection vial (Corning #CLS430791) and a stainless-steel tube with a 4 mm diameter opening.

The IMP samplers were mounted on a tripod 2 m above ground level to approximate the height of the switchgrass panicles, the open flower structures that produce pollen. The IMPs sampled airborne particles at a rate of 0.6 L/min, with collected particles entrained in sterile 15 mL conical tubes containing 2 mL of sterile deionized water.

2.2.4 Drone-based low-volume sampler (DRN)

To measure airborne pollen concentration at different altitudes above and downwind of the field, we used a drone-based sampling system consisting of the IMP unit mounted on a DJI Inspire 2 drone platform (Figure 3D). The system is described in detail in Bilyeu et al. (2022).

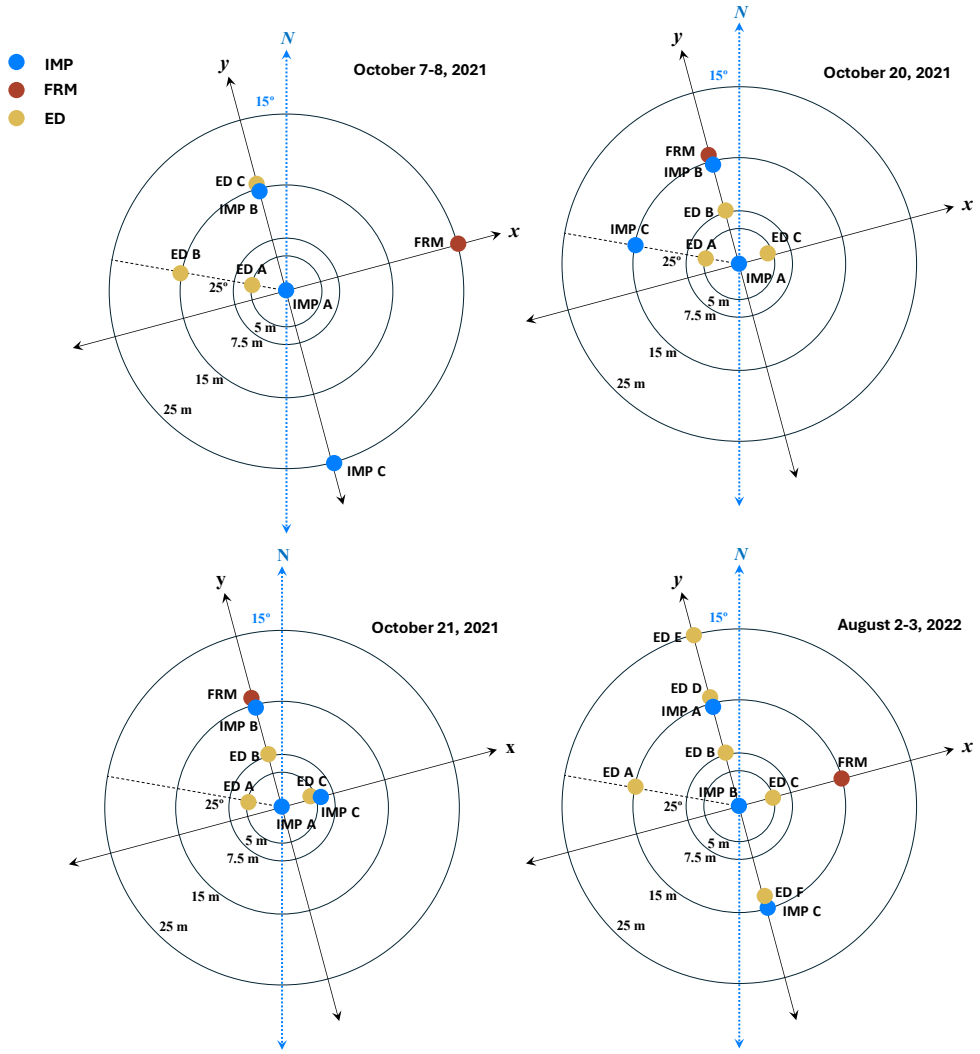

Figure 2. Ground-based sampler locations for each collection day. Yellow, blue, and red denotes placement of ED, IMP, and FRM samplers, respectively, positioned at radii of 5, 7.5, 15, and 25 meters from the center of field.

A key design feature of the drone system is the positioning of the IMP sampler high enough above the propellers, which ensures that the sampled air remains free from propeller-induced turbulence, commonly known as downwash. The drone was flown at a fixed altitude of 10 meters during each sampling interval, a height selected to prevent propeller downwash from disturbing the switchgrass canopy during stable hovering.

Due to drone battery limitations and the need for safe flight and landing operations, each sampling interval was restricted to 10 minutes. The IMP unit on the drone operated at the same volumetric sampling rate as its ground-based counterpart (0.6 L/min). However, because the drone sampler was only flown for 10 minutes per flight, its total sampling capacity was significantly lower than the ground-based IMP units, which collected for 30 to 90 minutes during the field campaign.

Hereafter, the IMP-equipped drone system is referred to as “DRN” throughout the manuscript.

2.3 Meteorological Data

A weather station was installed near the field to collect meteorological data throughout each sampling day. The station consisted of a Campbell Scientific CSAT3 three-dimensional sonic anemometer, mounted at a height of 1.5 m above ground level, which measured high-resolution wind velocity in three dimensions and sonic temperature at a frequency of 10 Hz. In addition, a Campbell Scientific HMP45C probe recorded temperature and relative humidity every 30 seconds. Meteorological data were recorded with the Campbell Scientific CR3000 datalogger. To minimize interference from the tripod pole, the sonic anemometer arm was positioned perpendicular to the anticipated dominant wind direction before each collection day. The wind velocities in the u and v directions (relative to the sonic anemometer arm) were then rotated into the cardinal coordinate system for analysis.

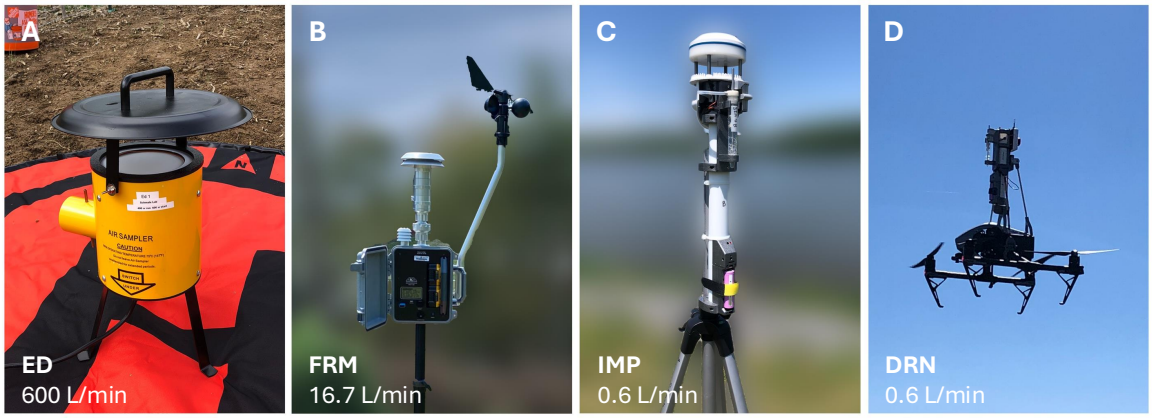

Figure 3. All sampler units used during the field campaigns. (A) The ED(Science First, 2007), a ground-based high-volume sampler (600 L/min). (B) The FRM, a ground-based medium-volume volumetric sampler (16.7 L/min). (C) The IMP, an impinger-based ground-based low-volume sampler (0.6 L/min). (D) The DRN, a drone-based sampler flown at a height of 10 meters above ground-level (0.6 L/min).

2.4 Processing of pollen samples

2.4.1 Sample preparation

Filters from the ED samplers were processed as shown in Figure 4A. Briefly, the 125mm "ED" collection filters were removed with forceps and transferred to separate 150 mm petri dishes (Fisher #FB0875714) in the field immediately following each sampling period. For each filter, 25 mL of 25% EtOH was added in the petri dish, the filter was gently agitated with a sterile cell spreader, and then rinsed a total of 8 times. Each rinsate was transferred by a pipettor to a vacuum filtration unit (Fisher Scientific #300-4100) containing a 47 mm Isopore polycarbonate 10μm filter (Millipore Sigma #TCTP04700). The sample was cleared through the filter using the vacuum from a hand pipetting bulb. Using forceps, the Isopore filter was then moved to a 60mm petri dish (Genesee 32-105) and rinsed 6 times with 2 mL 25% EtOH. The resulting rinsate was transferred to an Ultrafree 5 μm PVDF centrifugal filtration tube (Millipore Sigma UFC40SV25) and centrifuged for 2 minutes at 2,500 rpm in a swinging bucket centrifuge (IEC Clinical Centrifuge). The concentrated sample was then resuspended from the 5μm filter surface with 200μL 25% EtOH and moved to a 1.5 mL Eppendorf tube and stored at 4 °C for further analysis

Filters from the FRM sampler were processed as shown in Figure 4B. Briefly, the Isopore filter was removed from the FRM unit sampling cartridge using forceps and transferred to a 60 mm petri dish (Genesee 32-105) in the field immediately following each sampling period. For processing the sample, the Isopore filter was then rinsed 6 times with 2mL 25% EtOH, and the resulting rinsate was moved to an Ultrafree 5m PVDF centrifugal filtration tube (and centrifuged for 2 minutes at 2,500 rpm in a swinging bucket centrifuge (IEC Clinical Centrifuge). The concentrated sample was then resuspended from the 5m filter surface with 200 L of 25% EtOH and moved to a 1.5 mL Eppendorf tube and stored at 4 °C for further analysis.

The fluid from the IMP and DRN samplers was processed as shown in Figure 4C. Samples from the IMPs and DRN were transferred by pipette to an Ultrafree 5μm PVDF centrifugal filtration tube and centrifuged for 2 minutes at 2,500 rpm in a swinging bucket centrifuge (IEC Clinical Centrifuge). The concentrated sample was then resuspended from the 5 μm filter surface with 200 μl 25 EtOH and transferred to a 1.5 mL Eppendorf tube and stored at 4 °C for further analysis.

2.4.2 Pollen counting

Switchgrass pollen was counted in each concentrated sample by pipetting the samples into individual wells of a 96-well plate (Grenier Bio One 7000124). Samples were allowed to sediment for 15 minutes and then were observed using an Olympus CKX53 inverted microscope equipped with the Olympus EP50 digital camera and associated software. Following the quantification of the switchgrass pollen in each of the tubes, the samples were transferred back into their respective 1.5 mL Eppendorf storage tubes and held at 4 °C for transport and further analysis.

2.5 Atmospheric dispersal modeling

2.5.1 Meteorological Inputs

Atmospheric dispersal simulations for each sampling interval are driven using time-averaged wind statistics collected during that interval. Most sampling intervals occurred under low-wind conditions ($<$ 2 m/s), characterized by meandering winds with

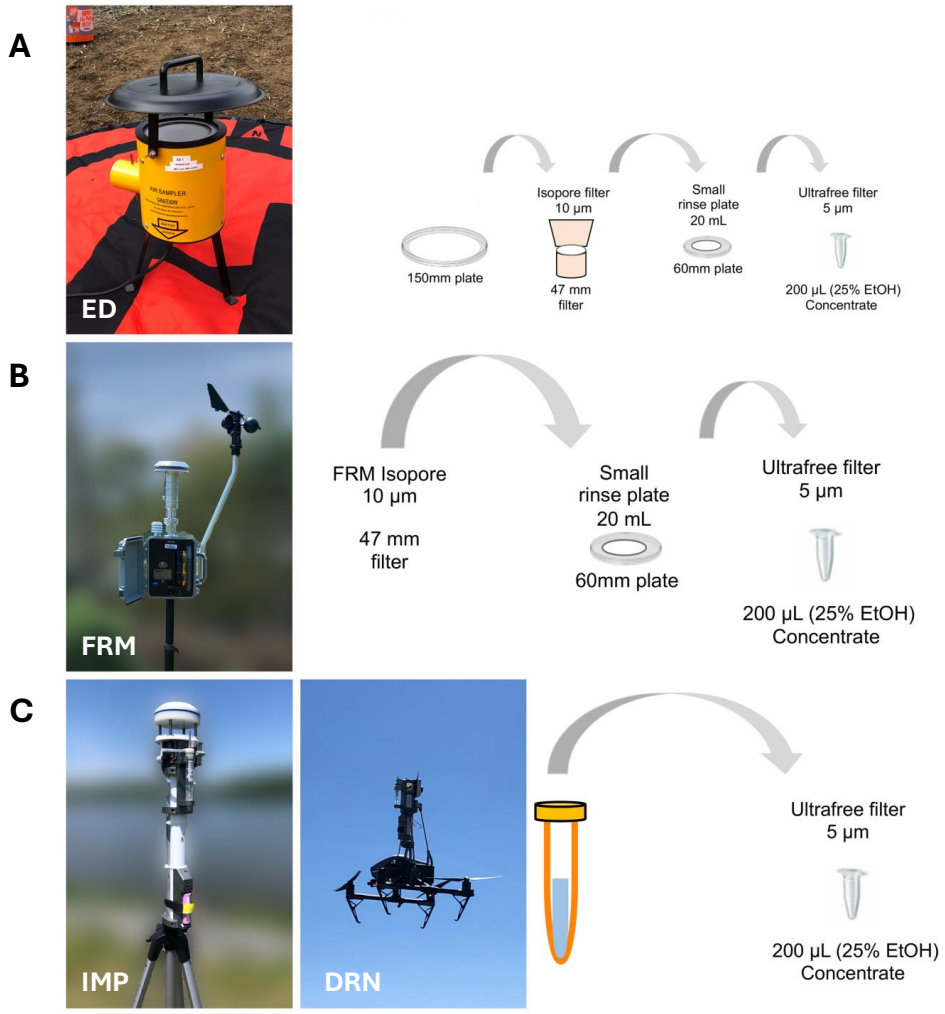

Figure 4. Flow charts showing the processing of the filters from (A) the ED samplers, (B) the FRM sampler, and (C) the IMP and DRN samplers.

frequent directional shifts and intermittent lulls in wind speed. To better capture dispersal dynamics under these conditions, the wind data was processed using different averaging window sizes. Specifically, for the 45-minute sampling intervals on August 2-3, 2022, the following averaging windows were used: 45 one-minute averaging windows, 9 five-minute averaging windows, and 1 full 45-minute averaging window. This approach allowed for assessing how different temporal resolutions of wind averaging influenced the accuracy of dispersal simulations.

To compute turbulence statistics for each averaging window, the average downwind direction was determined and the wind velocity data was rotated into the downwind (u)and crosswind (v) coordinate system. For each sampling interval, the means, covariances, and variances were computed for these wind velocity components, as well as temperature. Mean temperature was computed from sonic temperature using the method described in Schotanus et al. (1983) and the relative humidity values. Heat flux was estimated from sonic temperature and relative humidity using the Bowen ratio method from Schotanus et al. (1983). The Bowen ratio was determined using the simplified method of Lin et al. (2016), which requires only mean temperature and relative humidity. These turbulence statistics provided the necessary meteorological inputs for the dispersal simulation in each interval, specifically friction velocity (u^*) and the Monin-Obukhov length (L).

2.5.2 Pollen dispersal simulations

To simulate switchgrass pollen dispersal, we use the surface-layer Lagrangian Stochastic (LS) model described in Aylor and Flesch (2001) and expanded to three-dimensional transport in Aylor (2017). The LS model framework is based on Brownian motion theory, modeling turbulent diffusion by simulating the trajectories of thousands of particles through the air as random

walks through the atmosphere. The movement of each particle is governed by turbulent wind statistics, and the ensemble average of these trajectories provides estimates of pollen concentration at any given location within the simulation domain.

LS models require turbulence wind statistics to be specified at every point in the simulation domain, including mean velocities, variances, and covariances of the wind components. Under the assumptions of stationarity and horizontal homogeneity, these wind field statistics remain constant over time within each averaging window but vary with height. To account for this height dependence, boundary layer scaling techniques are applied to generate vertical wind profiles based on measurable surface-level parameters, specifically the friction velocity (u^*) and the Monin-Obukhov length (L). The full model formulation and wind statistics used in the simulations are provided in the code provided online.

These two parameters (u^* and L) were computed from the time-averaged meteorological measurements for each 45-minute sampling interval, using three different averaging approaches: one 45-minute averaging window; nine 5-minute averaging windows; and forty-five 1-minute averaging windows. A separate simulation was conducted for each averaging window in a 45-minute sampling interval, using the computed average wind direction, friction velocity (u^*), and Monin-Obukhov length (L). The resulting concentration fields from these simulations were then averaged to generate a single mean concentration field for each 45-minute sampling interval.

In each simulation, 100,000 particles (representing switchgrass pollen) are released from a point source at the center of the field at a height of 2 m, which approximates the height of most of the switchgrass panicles in the field experiment. Particles were removed from the simulation domain when they: traveled more than 50 m laterally from the source; rose above 100 m above ground level; or fell below 0.1 m above ground level. To simplify the simulation, pollen dispersion was modeled as if it occurred over a flat, rough surface, with estimated surface roughness of 0.01 m, consistent with values reported for level grassy plains and prairie in Hansen (1993). The settling velocity was estimated as **0.0371** m/s, based on an observed switchgrass pollen diameter of $\sim$35 μm, using Stokes' law. Since switchgrass pollen was observed to be nearly spherical, Stokes' law provides a reliable approximation of its settling velocity.

2.5.3 Concentration estimation and source emission rate calculation

The pollen concentration estimation procedure in this study follows the approach described by Flesch et al. (1995) for a stationary LS model with a constant source. Pollen concentration is estimated by tracking the amount of time particles spend in each grid box, normalized by the total number of particles released (N_p) and the volume of the grid box (V_box = 1 m $\times$ 1 m $\times$ 1 m), and then multiplied by the modeled emission rate (Q). Specifically, the concentration at a given grid point (i, j, k) is calculated as,

$$C(i,j,k) = Q\frac{1}{V_\mathrm{box}}\frac{1}{N_\mathrm{p}}\sum_{n=1}^{N_\mathrm{p}} T_n(i,j,k), \tag{1}$$

where $T_n(i, j, k)$ represents the time particle n spends in the given grid box.

We employed a model-measurement fusion approach described in Aylor and Flesch (2001) to estimate pollen emission rate and concentration. For each sampling interval, the modeled pollen concentration at each grid point in the simulation domain is first computed under the arbitrary assumption of a constant release rate at the center of the field of Q_model = 1 particle per second. This yields a modeled relative concentration, which is proportional to the actual concentration at every point in the domain. To estimate the actual emission rate (pollen flux from the field), the ratio of the measured pollen concentration at each of the six ED samplers to the modeled relative concentration at the corresponding locations in the simulation domain was computed and used to update the value of Q. To obtain a single emission rate estimate for each sampling interval, the computed emission rates corresponding to calculations based on each of the six ED samplers were averaged. This estimated true emission rate was then used to update the modeled relative concentration to predict the actual concentration at every point within the simulation domain.

To investigate dispersal at greater distances—up to 1 km from the source—the same modeling procedure is conducted but with a coarser grid resolution of V_box = 3 m $\times$ 3 m $\times$ 1 m and an extended simulation domain covering 1000 m $\times$ 1000 m $\times$ 100 m. This coarser grid was selected to balance computational efficiency while maintaining consistency with the finer-resolution near-source grid.

To generate 2D dispersal kernels, which represent pollen concentration as a function of distance, concentrations at equal radial distances from the source are averaged, yielding average concentration as a function of radial distance from the source.

3 Results

Three field campaigns were conducted over the course of two calendar years (2021 and 2022) to sample airborne pollen around two blocks of transgenic switchgrass.

3.1 Field Experiments

3.1.1 First campaign (October 7-8, 2021)

The first field campaign took place on October 7-8, 2021. At this time, the pANIC10A and PSYBIN1a plants (Fig. 1) were only 11 and 6 weeks old, respectively, and the youngest 200 pANIC10A plants had not yet been planted. The following ground based samplers were placed radially around the field at distances of 0, 5, 15, and 25 meters, as shown in figure 2: three ED samplers, three IMPs, and one FRM sampler. These ground-based samplers operated in 30-minute intervals, while the drone-based sampler (DRN) was flown at a 10-meter height for a duration of 10 minutes per sampling interval. However, due to technical difficulties, the drone sampler was only deployed on October 7th, and was not used on October 8th.

IMP A was placed at the center of the field (the midpoint of field 1 and 2) to estimate pollen emission rate, but an insufficient amount of pollen was collected—at most two pollen grains in each sampling interval, and often zero—which was not statistically significant to estimate the pollen emission rate. IMP B and ED C were co-located to verify alignment of their concentration estimates. However, due to their vastly different sampling rates and the low pollen numbers collected, direct comparisons were not feasible. On October 8th, slightly more pollen was captured, particularly by ED C, but overall pollen collection remained low. Impingers showed an increase in measured concentrations later in the afternoon, though data remained sparse. The IMP, FRM, and DRN samplers captured negligible pollen amounts.

Pollen concentrations for each sampling interval and sampler are presented in Table 1. On October 7th, too few pollen grains were collected for meaningful analysis. Concentrations marked with a dagger†superscript denote cases where only 1-2 pollen grains were sampled. On October 7th, all samplers captured 2 or fewer pollen grains. On October 8th, 1-5 grains were collected per sampler. IMP B did not capture any pollen, despite being placed alongside ED C, likely due to the overall low pollen counts.

3.1.2 Second campaign (October 20-21, 2021)

During the second field campaign on October 20-21, 2021, we increased ground-based sampling intervals to 90 minutes to compensate for the low pollen counts observed during the previous campaign's 30-minute sampling intervals. To improve pollen capture, all samplers were moved within 15 meters of the field. The drone was still flown for 10 minutes per sampling interval. On October 21st, heavy rainfall forced us to shorten the final sampling interval of the day. Despite the longer sampling durations and closer sampler placement, pollen counts remained negligible (at most two pollen grains captured per interval) throughout this campaign. See Table 1 for details.

3.1.3 Third campaign (August 2-3, 2022)

The third and final campaign took place on August 2-3, 2022. Field and sampler placements during this campaign are shown in Figure 1A and B, respectively. The oldest pANIC10A plants were at peak pollen production during this campaign, but the PSYBIN1a plants had not yet begun releasing pollen. The youngest pANIC10A field, planted only six weeks prior, was too immature to release pollen. Given that ED samplers were the most effective in previous campaigns, their number was increased from three to six. In anticipation of prevailing winds directed toward north-northeast, samplers were primarily aligned along the x and y axes in Figures 1 and 2. The drone sampler was again flown for 10 minutes at 10 meters during all sampling intervals. ED D and IMP A were co-located to compare concentration measurements. IMP B was placed at the field center to estimate the pollen emission rate, if sufficient pollen was collected. To address diurnal trends, sampling intervals were kept consistent across both collection days. All ground-based samplers were operated for 45-minute sampling intervals. ED samplers collected significantly more pollen than in previous campaigns. A clear diurnal pattern emerged, with concentrations peaking between 2:00-2:45 PM time on both days. Concentrations began increasing around 1:00 PM, peaked at 2:00 PM, then declined after 3:00 PM. See Table 1 for details.

3.2 Orange-Fluorescent Protein Expression

The primary source of pollen in the field experiments came from the first planted block of GE switchgrass, which contained 100 plants expressing OFP under the control of a maize ubiquitin promoter (PvUBI1). As shown in Figure 5, the OFP signal in pollen grains from these transgenic plants was difficult to distinguish from wildtype (WT) pollen exposed to the same OFP-inducing wavelength of light. In contrast, the OFP signal in pollen from the later planting of GE switchgrass (expressing OFP under a maize pollen-specific promoter, Zm13) was much stronger and easily distinguishable from WT pollen. However, these Zm13-expressing plants were smaller and did not produce sufficient mature panicles in time for the field experiments, limiting their contribution to the study.

3.3 Modeling Results

For the dispersal modeling, we focused on the third field campaign (August 2-3, 2022), as sufficient pollen was captured on both days to allow for concentration measurements from the ED samplers. All sampling intervals during these days were 45 minutes long. Sampling occurred at consistent times across both days, facilitating comparisons and enabling the identification of diurnal trends.

		ED						FRM	IMP			DRN**
Date	Time	A	B	C	D	E	F		A	B	C	
10/7/21	11:30-12:00	0	0.17	0	-	-	-	0	0	-	0	0
	12:35-13:05	0	0	0.06†	-	-	-	0	0	0	0	0
	13:45-14:15	0.06†	0	0	-	-	-	0	0	0	0	0
	14:45-15:15	0.11†	0	0.11†	-	-	-	2.00†	0	0	0	0
	15:50-16:20	0.17	0.06†	0.11†	-	-	-	0	0	0	0	0
10/8/21	12:00-12:30	0	0	0.33	-	-	-	2.00†	0	0	0	-
	13:00-13:30	0.17	0.17	0.06†	-	-	-	0	0	0	0	-
	14:00-14:30	0	0	0.22	-	-	-	0	111.11†	0	0	-
	15:00-15:30	0.11†	0.17	0.33	-	-	-	0	0	0	0	-
10/20/21	14:00-16:00*	0.02†	0.02†	0.02†	-	-	-	0.67†	0	0	0	0
	16:30-18:15*	0.02†	0.02†	0.02†	-	-	-	0	0	0	0	0
10/21/21	12:00-13:45*	0	0	0.02†	-	-	-	0	0	0	0	0
	14:00-14:50	0	0	0.03†	-	-	-	0	0	0	0	0
8/2/22	10:00-10:45	0.37	0.48	2.48	0.15	0.04†	0.04†	0	0	0	0	0
	11:00-11:45	0.11	0.89	0.59	0.04†	0.04†	0.04†	0	0	0	0	0
	12:00-12:45	0.07†	3.19	1.04	0.37	0.22	0.11	0	0	0	0	0
	13:00-13:45	0.22	4.30	31.78	0.33	0.26	1.89	0	0	0	0	-
	14:00-14:45	0.37	41.44	19.74	4.67	1.00	1.59	15.97	74.07†	37.04†	0	166.67†
	15:00-15:45	0.26	5.41	5.85	0.15	0.11	0.22	3.99	0	0	37.04†	0
8/3/22	10:00-10:45	0.04†	0.15	0.33	0	-	0.07†	0	0	37.04†	0	333.33†
	11:00-11:45	0	1.74	0.30	0.07†	0	0.15	0	0	0	0	0
	12:00-12:45	0	0.48	0.85	0.04†	0.15	0.07†	0	0	0	0	0
	13:00-13:45	0.15	6.22	17.89	0.74	0.04†	0.11	1.33†	0	37.04†	37.04†	0
	14:00-14:45	15.11	23.44	29.26	9.67	1.70	3.19	10.65	0	444.44	74.07†	500.00
	15:00-15:45	0.78	5.19	9.07	1.44	-	0.48	13.31	111.11	185.19	37.04†	0

Table 1. Pollen concentrations (pollen/m^3) sampled during specific time periods, organized by date and sampler type.
†Only 1-2 pollen grains were sampled.
*sampling times for ED and FRM were limited to two 45 minute intervals with a break in between to prevent overheating, resulting in 90 minutes of total sampling time. Impingers sampled for the entire time.
**drone was sampling for 10 minutes in every interval due to battery limitations

3.3.1 Near-source concentration and emission rate estimation

Dispersal simulations more accurately capture changing wind directions and pollen concentrations when shorter averaging periods are used for each sampling interval. Figure 6 presents ground-level relative concentration contours and downwind wind roses for the August 2nd, 2:00-2:45 PM sampling interval, simulated using 1-minute, 5-minute, and 45-minute averaging windows. This interval corresponded to the highest measured pollen concentrations by the ED samplers. The wind rose in Figure 6A was generated using wind data collected at a sampling frequency of 10 Hz. The wind roses in Figure 6B, C, and D were created using 1-minute, 5-minute, and 45-minute time-averaged wind data, respectively. Wind roses display the downwind direction. Yellow circles indicate the ED sampler locations, with their size proportional to pollen counts at each site.

Comparison of averaging windows. The 45-minute plot (Figure 6D), based on a single LS simulation in the average downwind direction, fails to capture wind variability and lateral pollen spread, missing high pollen counts at ED sampler B due to a single eastward-directed plume. The 5-minute plot (Figure 6C), which averages nine LS simulations, shows some directional variation but lacks the detail seen in the 1-minute plot. The 1-minute plot (Figure 6B) provides the most accurate representation of dispersal dynamics. However, all three simulations share a common discrepancy: peak concentrations appear a few meters from the point source, indicating lateral transport before deposition. A field source, rather than a point source, may better address these inconsistencies, at the cost of further model complexity.

Emission rate and diurnal pattern. The computed pollen emission rate from the field exhibits a clear diurnal trend. Figure 7 presents the mean, minimum, and maximum non-zero computed emission rates for each sampling interval on August 2-3, 2022 during the third field campaign. Emission rates were computed from Equation (1), based on the ratio of measured to modeled concentrations. Samplers with zero measured or modeled concentrations were excluded to prevent infinite or zero emission rate estimates. Emission rate calculations were performed for 1-minute, 5-minute, and 45-minute averaging windows. The range

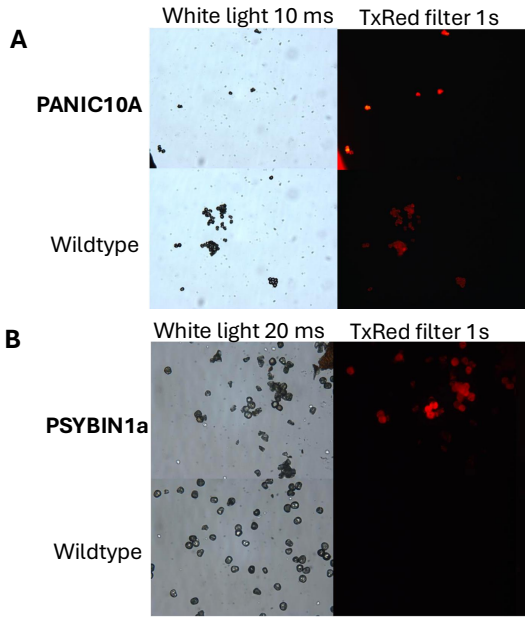

Figure 5. Comparison of OFP signal between GE switchgrass pollen and wildtype. (A) Pollen from the pANIC10A strain (OFP expression throughout the entire plant) is not easily distinguishable from wildtype pollen under OFP-inducing light. (B) Pollen from the PSYBIN1a strain (OFP expression restricted to pollen) exhibits a strong, highly distinguishable OFP signal compared to wildtype pollen.

of estimated emission rates decreases with smaller averaging windows, indicating greater precision with shorter averaging periods. The pollen emission rate increased by approximately three orders of magnitude between 10 AM and 2 PM. Note that the emission rate is shown on a log scale in Figure 7. The log-transformed emission rate estimate is positively correlated with the horizontal velocity magnitude (Pearson's R = 0.73, P = 0.01), temperature (R = 0.71, P = 0.01), and vapor pressure deficit (R = 0.69, P = 0.01), while negatively correlated with relative humidity (R = -0.63, P = 0.02). These results indicate that higher pollen emissions occur under conditions of higher wind speed, temperature, and vapor pressure deficit, while increased relative humidity reduces pollen release.

Modeled concentration predictions improve dramatically when changing wind conditions are incorporated into the simulations. Figure 8 compares modeled concentrations, computed by multiplying the estimated emission rate by the relative concentration, with measured concentrations derived from ED sampler pollen counts. Although the figures directly compare modeled and measured concentrations, they are not intended as a formal model validation, as the measured concentrations were directly used to compute emission rate and modeled concentration (see Section 2.5.3). Instead, they highlight the substantial improvement in model performance as the averaging window is reduced. The Pearson's R-value increases from 0.19 for 45-minute windows to 0.71 for 5-minute windows to 0.84 for 1-minute windows. While reducing the averaging window from 45 minutes to 5 minutes requires nine times the computational power, it yields a 270% improvement in model performance (as measured by the R-value). In contrast, refining the resolution further from 5-minute to 1-minute windows results in only a 20% increase, suggesting that shorter windows may not always be computationally worthwhile beyond a certain threshold.

3.3.2 Estimating sensor capabilities in the far field

The intake rates of the samplers used in this study differ by multiple orders of magnitude, with 0.6 L/min for the low-volume IMP and DRN, 16.7 L/min for the medium-volume FRM, and 600 L/min for the high-volume ED. This disparity highlights the coarseness of concentration measurements for the low-volume IMP and DRN samplers, particularly when considering error estimates based on the Poisson distribution. The Poisson distribution models the error of discrete event counts, such as the number of pollen grains collected, as $\sqrt{N}$, where N is the number of pollen grains captured by a sampler (Addison-Smith et al., 2020; Lin et al., 2013). Lower intake rates necessitate proportionally higher aerial concentrations, and consequently, greater pollen emission rates for detection, leading to significantly higher measurement error compared to high-volume samplers.

To determine optimal sampler placement based on varying field emission rates, we combined sampler intake rates with long-distance dispersal simulations. Figure 9 plots the maximum distances at which each sampler could be placed to collect at least 100 pollen grains (± 10) within a 45-minute sampling interval, as a function of the pollen emission rate. These estimates

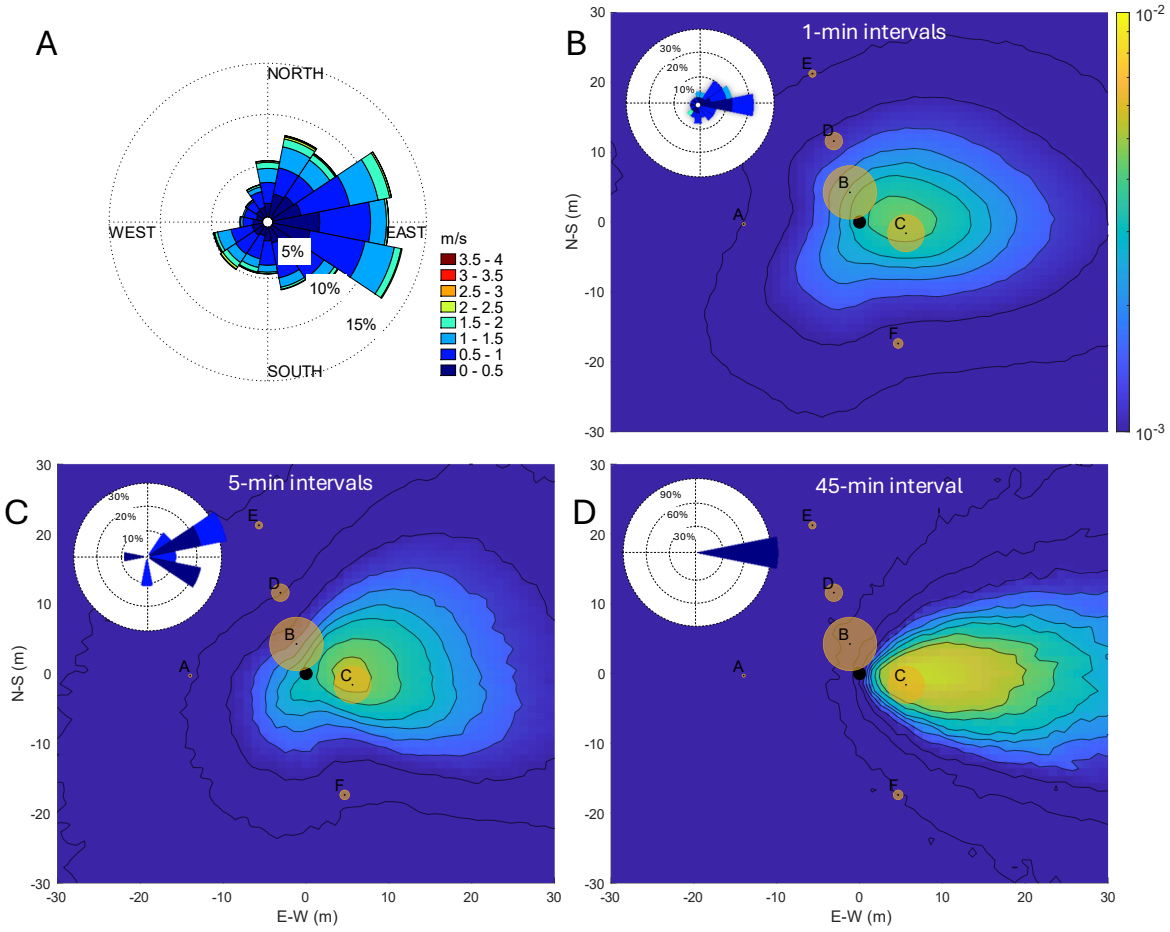

Figure 6. Relative ground-level concentration contours for the August 2nd, 2:00-2:45 PM sampling interval. (A) Wind rose for this sampling interval, indicating the downwind direction. (B) Contour plot averaging forty-five 1-minute simulations. (C) Contour plot averaging nine 5-minute simulations. (D) Contour plot generated using a single 45-minute simulation. Yellow circles indicate the ED sampler locations, with their size proportional to pollen counts at each site.

were generated using the long-distance 2D relative concentration dispersal kernels, computed separately for ground-based samplers (IMP, ED, FRM) at ground level and the drone-based sampler (DRN) at 10 m above ground level. Although the drone was only flown for 10 minutes per sampling interval in our field campaigns, we evaluated its performance over 45-minute intervals to account for potential future battery-life improvements or wire-tether power modifications. The threshold of 100 pollen grains corresponds to different effective concentrations across sampler types, with 3.7×10^3 pollen/m^3 for IMP and DRN, 133 pollen/m^3 for FRM, and 3.7 pollen/m^3 for ED. This threshold was selected as it ensures a $\pm 10\%$ error in concentration estimates when modeled with the Poisson distribution.

Figure 9 shows that, to collect at least 100 pollen grains, the ED samplers require 1.5 orders of magnitude less emission rate than the FRM and 3 orders of magnitude less than the IMP, across all distances from the field. This advantage allows ED samplers to be placed significantly farther from the field compared to IMP and FRM samplers. The DRN requires an even greater emission rate, due to lower concentrations at 10 meters altitude. However, at approximately 200 meters downwind, the DRN and IMP detection capabilities converge, as vertical concentration gradients become less pronounced further from the source.

The gray vertical lines in Figure 9 represent computed emission rate values at each ED sampler during our field campaign, which are also shown in Figure 7. These results indicate that only the ED samplers had a reasonable chance of collecting at least 100 particles during some sampling intervals. The remaining samplers were largely ineffective at detecting airborne pollen given the small emission rates observed in this study, even at close proximity to the source field. For a larger source, with an emission rate of 10^6 pollen/s (approximately 100 times larger than ours), the feasible placement of samplers would improve substantially. Under such conditions, impingers could be placed up to 10 meters from the field, the FRM samplers could be

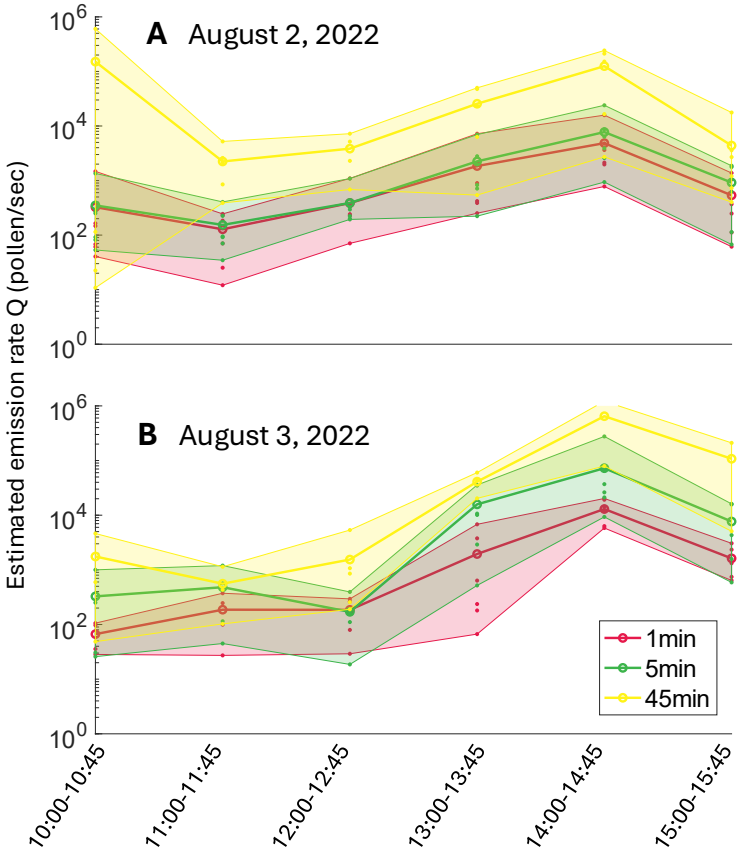

Figure 7. Mean estimated pollen emission rates for each sampling interval using 1-minute, 5-minute, and 45-minute simulations. (A) Estimated emission rates for August 2, 2022 and (B) August 3, 2022. Non-zero emission rate estimates for each sampler are shown as solid points. Shaded regions indicate the range the between minimum and maximum non-zero emission rate estimates. The vertical axis is on a log scale.

placed up to 100 meters from the field, and ED samplers could be placed up to 200 meters away. These adjustments would allow each sampler type to collect at least 100 pollen grains within a 45-minute sampling interval, enhancing measurement reliability and reducing uncertainty.

Discussion

In these field experiments, airborne pollen from two different strains of OFP-expressing switchgrass plants were captured and analyzed using the method described in (Rice et al., 2013). The PSYBIN1a strain exhibited strong fluorescence compared to wild-type pollen, whereas the pANIC10A strain was difficult to distinguish by fluorescence alone. However, since the PSYBIN1a plants did not release sufficient pollen during any of the field experiments, OFP expression was not used for pollen identification in this study. If we had successfully captured PSYBIN1a pollen from the younger field, it would have expedited the counting and sampling process. Despite this limitation, the study serves as a proof-of-concept that fluorescence tagging can be a valuable tool for pollen tracking. Though prior studies have tracked the movement of pollen in the atmosphere (Aylor et al., 2006; Aylor and Flesch, 2001; Aylor et al., 2003), to our knowledge, this is the first detailed study to incorporate aerial and ground-based volumetric samplers to track the movement of GE pollen from a known source. Fluorescent tagging presents a unique opportunity to trace pollen dispersal and track its movement over long distances. Understanding switchgrass gene flow is particularly relevant as biofuel production increases, helping to mitigate ecological risks posed by invasive strains and unintended cross-pollination between transgenic varieties (Kwit and Stewart, 2012). Additionally, fluorescence-tagged pollen could facilitate rapid and automated counting using instruments such as the Helmut Hund BAA500, Plair Rapid-E, or WIBS-4

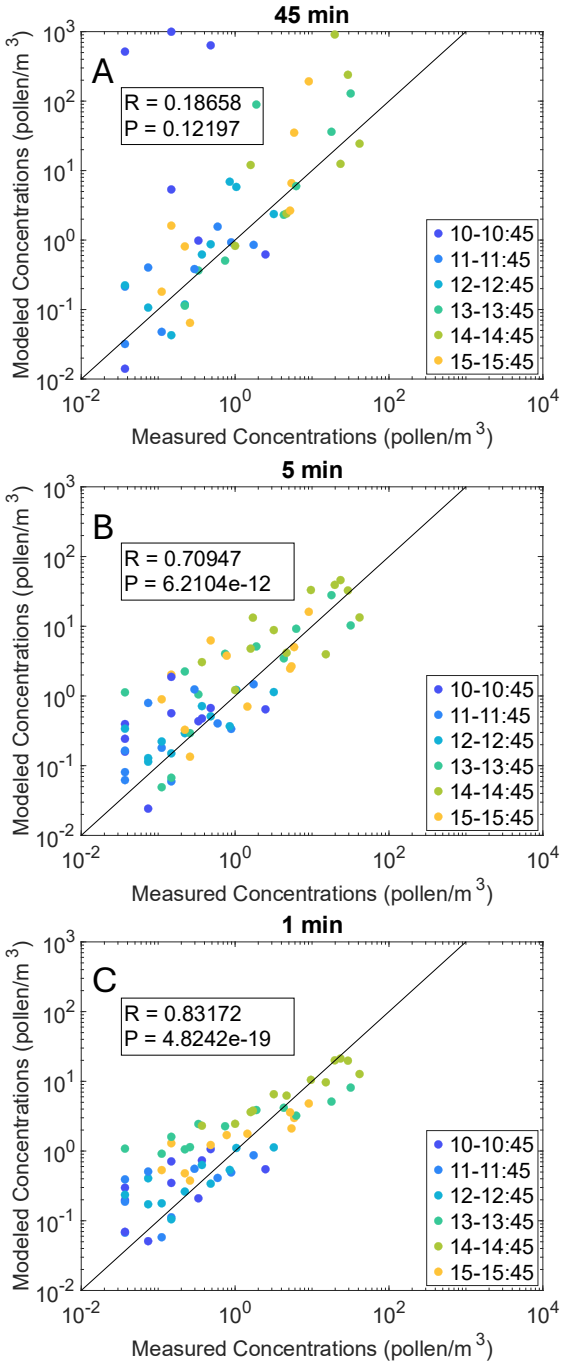

Figure 8. Measured concentrations at the ED samplers compared with simulated concentrations for (A) 45-minute, (B) 5 minute, and (C) one-minute intervals. These plots are not intended as model validation, but rather to show that decreasing the averaging time for simulations greatly improves modeled concentrations. Note that the plots are on log-log scales.

(Buters et al., 2024; O'Connor et al., 2014), which is of particular interest for allergen monitoring.

During the final campaign on August 2-3, 2022, a distinct diurnal pattern emerged in both measured pollen concentrations and computed pollen emission rate. Pollen emission rate increased steadily after the first sampling interval at 10 AM, peaked at 2 PM on both days, and declined during the final sampling interval at 3 PM. This diurnal pattern was consistent across both days and correlated with increasing wind velocity and temperature, as well as decreasing relative humidity. Such diurnal pollen release patterns are common in wind-pollinated species, where anther dehiscence is driven by drying conditions such as low

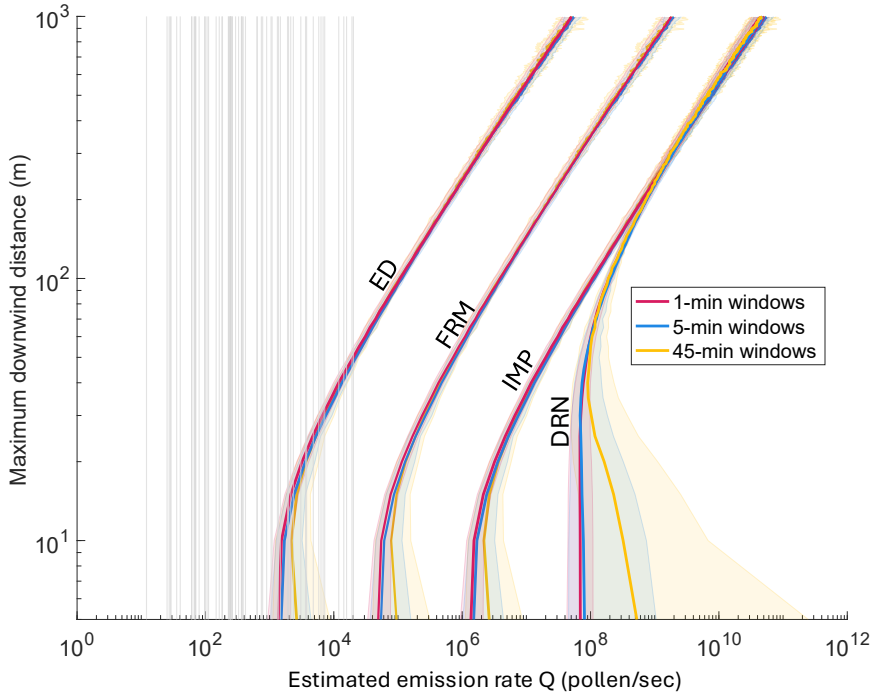

Figure 9. Maximum distance at which ED, FRM, IMP, and DRN sensors should be placed from the source to capture at least 100 pollen grains for a given a emission rate from the field. These are calculated using concentration curves derived from each sampling interval, distinguishing between estimates computed with 1-minute, 5-minute, and 45-minute averaging windows. Solid lines represent the median values, while the shaded regions indicate the range between the lowest and highest values observed across all sampling intervals. Gray vertical lines correspond to the estimated emission rates for each sensor during all sampling periods.

humidity and rising temperatures (Sofiev and Bergmann, 2012). Similar trends have been observed in previous switchgrass field studies, where peak pollen concentrations occurred in the late morning and early afternoon, followed by a decline around 3 PM (Auer et al., 2016). Comparable findings in maize have linked pollen release patterns to increasing vapor pressure deficit (Jarosz et al., 2005) and decreasing relative humidity combined with rising wind velocity (Marceau et al., 2011). This information can be used to better predict peak allergen concentrations and improve accuracy of large-scale air pollution models.

Throughout all sampling intervals and field campaigns, we observed very low wind velocities (< 2 m/s) and frequent shifts in wind direction. Under these meandering wind conditions, particle dispersal is primarily controlled by wind direction shifts rather than turbulence (Vickers et al., 2008; Anfossi et al., 2005). Standard dispersal models that assume a dominant downwind direction fail to account for this effect, often producing overly narrow plumes that underestimate lateral spread. This limitation is particularly characteristic of LS models (Jarosz et al., 2005; Anfossi et al., 1990) and Gaussian plume models (Sagendorf and Dickson, 1974) which require a single downwind direction. Even more advanced modeling approaches, such as Large Eddy Simulations, do not fully incorporate changing wind directions (Chamecki et al., 2009). To address this, we reduced the averaging window for wind statistics from 45 minutes to 5 and 1 minute, then ran dispersal models for each of these smaller intervals and combined the resulting plumes. This approach dramatically improved the fit between modeled and measured concentrations, enhancing emission rate estimates. Similar techniques have been applied in Gaussian plume modeling with 2-minute intervals, yielding significantly better agreement with measured data (Sagendorf and Dickson, 1974). Anfossi et al. (1990) (Anfossi et al., 1990) also emphasized the importance of using short averaging windows for dispersal modeling, recommending intervals of only a few minutes. A maize dispersal study similarly attributed discrepancies between measured and modeled concentrations to wind direction variability and assumptions of a dominant wind direction (Jarosz et al., 2005). Future large-scale pollen forecasting and bio-confinement strategies should consider meandering wind conditions, which are not currently accounted for in large-scale models (Chamecki et al., 2009).

The highest concentration measurements in this study came from the high-volume ED samplers. The pollen source size—100 plants releasing pollen—was exceedingly small compared to previous dispersal experiments in switchgrass, which

involved 3,200 plants (Auer et al., 2016), as well as studies in maize (Jarosz et al., 2005; Aylor et al., 2006; Marceau et al., 2011). High-volume ED samplers performed best under these small-source conditions, capturing spatial variations in concentration and diurnal patterns. To the best of our knowledge, this is the first pollen-trapping field study to utilize these samplers. Their volumetric flow rate of 600 L/min is 60 times greater than that of the traditional Hirst-type samplers, which operate at 10 L/min and are comparable to the FRM sampler used in this study. Due to the small pollen source, the FRM sampler did not produce usable data. As the ED samplers were originally designed for educational purposes, they are inexpensive and lack pre-programming and other advanced features found in commercial volumetric samplers. However, their simplicity and affordability make them easily deployable, and they have strong potential for measuring concentrations from small sources and capturing high-resolution pollen dispersal patterns even in small fields.

A novel impinger-type particle sampler (IMP and DRN) was used in this study to collect pollen, marking the first application of this integrated system for pollen tracking. While previously employed for airborne microbial sampling(Powers et al., 2018; Bilyeu et al., 2022), this study extends its use to pollen dispersal. The IMP and DRN samplers successfully collected pollen in the field, demonstrating their feasibility for tracking pollen movement. However, due to the small source size, limited pollen production, and the relatively low sampling rate of 0.6 L/min, the collected pollen quantities were insufficient for reliable concentration estimates. The differing flow rates between the ED and IMP samplers further complicate direct comparisons, as impinger samplers inherently capture fewer particles at high concentrations due to their small intake volumes. The IMP system would likely perform more effectively when sampling from much larger sources, at least 100 times the size of the field used in our study (Figure 9). Similarly, the drone-mounted sampler, operating at 10 m AGL, would require a significantly larger pollen source for effective deployment at further distances and altitudes. Nevertheless, the drone platform remains a valuable tool for aerobiological research, offering future opportunities for prolonged and spatially resolved sampling, particularly when paired with higher-volume sampling technologies, including those incorporating filter-based collection systems. Moreover, impinger samplers, which preserve particles in liquid, could prove especially useful for future viability and molecular studies.

Future studies would benefit greatly from a larger and stronger pollen source, which would enable long-distance tracking and strengthen the conclusions drawn from this study. The small source size in our current setup limited all measurements to within 20 meters of the field and prevented effective use of all but the highest-volume samplers (EDs). A substantially larger source would allow meaningful comparisons between low- and high-volume samplers, with one set used to estimate the particle release rate and another for validating modeled concentrations. It would also enable the use of impinger-type samplers (IMP and DRN), which can preserve pollen for downstream viability studies.

Focusing solely on PSYBIN1a switchgrass, with its stronger OFP fluorescence in pollen, could further enhance tracking accuracy via automatic fluorescence-based quantification. As shown in Figure 9, these methods could enable pollen detection up to 1 km or even tens of kilometers from the source. This fluorescence tagging technique could also be transferable to other crops of interest. For instance, hemp is known to produce copious amounts of pollen capable of long-distance dispersal, and its monitoring is increasingly relevant (Nimmala et al., 2024). If transgenic hemp lines become available, similar fluorescence-based tracking methods could be applied to study its pollen movement and gene flow in detail.

Conclusion

Three field campaigns were conducted to measure pollen concentrations around a small field of genetically modified switchgrass, utilizing both traditional and novel sampler types. The experiments also included a drone-mounted sampler, demonstrating the feasibility of airborne pollen sampling at 10 meters above the field as a proof-of-concept. Despite the exceedingly small source size, the high-volume ED samplers successfully collected sufficient pollen to analyze spatial variations in concentration and identify diurnal release patterns. This study evaluated the effectiveness of different sampler types for pollen collection under varying conditions. Among the three field campaigns, only the final campaign on August 2-3, 2022, produced sufficient concentration data for detailed analysis and modeling. During this campaign, a clear diurnal pattern was observed in the pollen concentration and, consequently, in the calculated emission rate. Persistent low-wind meandering conditions were recorded throughout the campaign, and reducing the averaging window for simulations significantly improved pollen emission rate estimations by better incorporating shifting wind directions. This study highlights the potential for drone-based pollen sampling and fluorescence-based GMO pollen tracking. The findings provide insight into the effectiveness of different sensor types with respect to source strength and sampling distance, advancing the understanding of pollen dispersal dynamics and measurement techniques. These results have important implications for allergen monitoring, cross-pollination risk assessment, and broader bioaerosol surveillance strategies.

Data and code availability

All sampling data, modeling code, and simulation results are made available in the Virginia Tech Data repository: https://figshare.com/s/54a3081

References

Adamov, S., Lemonis, N., Clot, B., Crouzy, B., Gehrig, R., Graber, M.-J., Sallin, C., and Tummon, F. (2024). On the Measurement Uncertainty of Hirst-Type Volumetric Pollen and Spore Samplers. *Aerobiologia*, 40(1):77–91.

Addison-Smith, B., Wraith, D., and Davies, J. M. (2020). Standardising Pollen Monitoring: Quantifying Confidence Intervals for Measurements of Airborne Pollen Concentration. *Aerobiologia*, 36(4):605–615.

Ahrens, C., Ecker, G., and Auer, C. (2011). The Intersection of Ecological Risk Assessment and Plant Communities: An Analysis of *Agrostis* and *Panicum* Species in the Northeastern U.S. *Plant Ecol.*, 212(10):1629–1642.

Ahrens, C. W., Meyer, T. H., and Auer, C. A. (2014). Distribution Models for *Panicum virgatum* (Poaceae) Reveal an Expanded Range in Present and Future Climate Regimes in the Northeastern United States. *Am. J. Bot.*, 101(11):1886–1894. Epub 2014 Oct 24; PMID: 25366854.

Anfossi, D., Brusasca, G., and Tinarelli, G. (1990). Simulation of Atmospheric Diffusion in Low Windspeed Meandering Conditions by a Monte Carlo Dispersion Model. *Nuovo Cim. C*, 13(6):995–1006.

Anfossi, D., Öttl, D., Degrazia, G., and Goulart, L. A. (2005). An Analysis of Sonic Anemometer Observations in Low Wind Speed Conditions. *Boundary-Layer Meteorol.*, 114(1):179–203.

ARA Instruments (2016). N-FRM Sampler. https://arainstruments.com/products/n-frm-sensor/. Product web page.

Auer, C., Meyer, T., and Sagun, V. (2016). Reducing Pollen Dispersal using Forest Windbreaks. *Plant Science Articles*, (28).

Aylor, D. E. (2017). *Aerial Dispersal of Pollen and Spores*. American Phytopathological Society, St. Paul, MN.

Aylor, D. E., Boehm, M. T., and Shields, E. J. (2006). Quantifying Aerial Concentrations of Maize Pollen in the Atmospheric Surface Layer Using Remote-Piloted Airplanes and Lagrangian Stochastic Modeling. *J. Appl. Meteorol. Climatol.*, 45(7):1003–1015.

Aylor, D. E. and Flesch, T. K. (2001). Estimating Spore Release Rates Using a Lagrangian Stochastic Simulation Model. *J. Appl. Meteorol. Climatol.*, 40(7):1196–1208.

Aylor, D. E., Schultes, N. P., and Shields, E. J. (2003). An Aerobiological Framework for Assessing Cross-Pollination in Maize. *Agric. For. Meteorol.*, 119(3-4):111–129.

Bilyeu, L., Bloomfield, B., Hanlon, R., González-Rocha, J., Jacquemin, S. J., Ault, A. P., Birbeck, J. A., Westrick, J. A., Foroutan, H., Ross, S. D., Powers, C. W., and Schmale, D. G. (2022). Drone–Based Particle Monitoring above Two Harmful Algal Blooms (HABs) in the USA. *Environ. Sci.: Atmos.*, 2(6):1351–1363.

Buters, J. T. M., Antunes, C., Galveias, A., Bergmann, K.-C., Thibaudon, M., Galán, C., Schmidt-Weber, C., and Oteros, J. (2018). Pollen and spore monitoring in the world. *Clin. Transl. Allergy*, 8:9.

Buters, J. T. M., Clot, B., Galán, C., Gehrig, R., Gilge, S., Hentges, F., O'Connor, D., Sikoparija, B., Skjoth, C., and Tummon, F. (2024). Automatic Detection of Airborne Pollen: An Overview. *Aerobiologia*, 40(1):13–37.

Chamecki, M., Meneveau, C., and Parlange, M. B. (2009). Large eddy simulation of pollen transport in the atmospheric boundary layer. *J. Aerosol Sci.*, 40(3):241–255.

Ecker, G., Meyer, T., and Auer, C. (2013). Pollen longevity and dispersion models for switchgrass. *Crop Sci.*, 53(3):1120–1127.

Ecker, G., Zalapa, J., and Auer, C. (2015). Switchgrass (*Panicum virgatum* l.) genotypes differ between coastal sites and inland road corridors in the Northeastern US. *PLoS One*, 10(6):e0130414.

Flesch, T. K., Wilson, J. D., and Yee, E. (1995). Backward-time Lagrangian stochastic dispersion models and their application to estimate gaseous emissions. *J. Appl. Meteorol. Climatol.*, 34(6):1320–1332.

Gottwald, T. R. and Tedders, W. L. (1985). A spore and pollen trap for use on aerial remotely piloted vehicles. *Phytopathology*, 75(7):801–807.

Hansen, F. V. (1993). *Surface roughness lengths*. US Army Research Laboratory.

Isard, S. A. and Gage, S. H. (2001). *Flow of Life in the Atmosphere*. Michigan State University Press.

Jarosz, N., Loubet, B., Durand, B., Foueillassar, X., and Huber, L. (2005). Variations in maize pollen emission and deposition in relation to microclimate. *Environ. Sci. Technol.*, 39(12):4377–4384.

Kausch, A. P., Hague, J., Oliver, M., Li, Y., Daniell, H., Mascia, P., Watrud, L. S., and Stewart, C. N. (2010). Transgenic perennial biofuel feedstocks and strategies for bioconfinement. *Biofuels*, 1(1):163–176.

Kwit, C. and Stewart, C. N. (2012). Gene flow matters in switchgrass (*Panicum virgatum* L.), a potential widespread biofuel feedstock. *Ecol. Appl.*, 22(1):3–7.

Li, R. and Qu, R. (2011). High throughput agrobacterium-mediated switchgrass transformation. *Biomass Bioenergy*, 35(3):1046–1054.

Lin, B., Bozorgmagham, A., Ross, S. D., and Schmale III, D. G. (2013). Small fluctuations in the recovery of fusaria across consecutive sampling intervals with unmanned aircraft 100 m above ground level. *Aerobiologia*, 29:45–54.

Lin, K., Juang, J., Shiu, Y.-W., and Chang, L. (2016). Estimating the Bowen ratio for application in air quality models by integrating a simplified analytical expression with measurement data. *J. Appl. Meteorol. Climatol.*, 55(4):1041–1048.

Mann, D. G. J., LaFayette, P. R., Abercrombie, L. L., King, Z. R., Mazarei, M., Halter, M. C., Poovaiah, C. R., Baxter, H., Shen, H., Dixon, R. A., Parrott, W. A., and Stewart, C. Neal, J. (2012). Gateway-compatible vectors for high-throughput gene functional analysis in switchgrass (*Panicum virgatum* L.) and other monocot species. *Plant Biotechnol. J.*, 10(2):226–236. Epub 2011 Sep 28; PMID: 21955653.

Marceau, A., Loubet, B., Andrieu, B., Durand, B., Foueillassar, X., and Huber, L. (2011). Modelling diurnal and seasonal patterns of maize pollen emission in relation to meteorological factors. *Agric. For. Meteorol.*, 151(1):11–21.

Millwood, R., Nageswara-Rao, M., Ye, R., Terry-Emert, E., Johnson, C. R., Hanson, M., Burris, J. N., Kwit, C., and Stewart, C. N. (2017). Pollen-mediated gene flow from transgenic to non-transgenic switchgrass (*Panicum virgatum* L.) in the field. *BMC Biotechnol.*, 17:1–10.

Nimmala, M., Ross, S. D., and Foroutan, H. (2024). *Cannabis* pollen dispersal across the United States. *Sci. Rep.*, 14(1):20605.

O'Connor, D. J., Healy, D. A., Hellebust, S., Buters, J. T., and Sodeau, J. R. (2014). Using the WIBS-4 (Waveband Integrated Bioaerosol Sensor) technique for the on-line detection of pollen grains. *Aerosol Sci. Technol.*, 48(4):341–349.

Parrish, D. J. and Fike, J. H. (2005). The biology and agronomy of switchgrass for biofuels. *Crit. Rev. Plant Sci.*, 24(5-6):423–459.

Plaza, M. P., Kolek, F., Leier-Wirtz, V., Brunner, J. O., Traidl-Hoffmann, C., and Damialis, A. (2022). Detecting airborne pollen using an automatic, real-time monitoring system: Evidence from two sites. *Int. J. Environ. Res. Public Health*, 19(4):2471.

Powers, C. W., Hanlon, R., Grothe, H., Prussin, A. J., Marr, L. C., and Schmale III, D. G. (2018). Coordinated sampling of microorganisms over freshwater and saltwater environments using an unmanned surface vehicle (USV) and a small unmanned aircraft system (sUAS). *Front. Microbiol.*, 9:1668.

Powers, C. (2018). Schmale-Lab-3D-Printing-Files-Powers-et-al-Frontiers-2018. GitHub repository. https://github.com/SchmaleLab/Schmale-Lab-3D-Printing-Files-Powers-et-al-Frontiers-2018.

Rice, J. H., Millwood, R. J., Mundell, R. E., Chambers, O. D., Abercrombie, L. L., Davies, H. M., and Stewart, C. N. (2013). An orange fluorescent protein tagging system for real-time pollen tracking. *BMC Res. Notes*, 6:1–7.

Sagendorf, J. F. and Dickson, C. R. (1974). Diffusion under low wind-speed inversion conditions. Technical memorandum erl arl-52, U.S. National Oceanic and Atmospheric Administration, Air Resources Laboratory, Silver Spring, MD.

Schmale III, D. G., Dingus, B. R., and Reinholtz, C. (2008). Development and application of an autonomous unmanned aerial vehicle for precise aerobiological sampling above agricultural fields. *J. Field Robot.*, 25(3):133–147.

Schotanus, P., Nieuwstadt, F., and De Bruin, H. (1983). Temperature measurement with a sonic anemometer and its application to heat and moisture fluxes. *Boundary-Layer Meteorol.*, 26:81–93.

Science First (2007). 15000 High Volume Air Sampler. PDF product sheet. https://sciencefirst.com/wp-content/uploads/2017/05/15000-High-Volume-Air-Sampler.pdf.

Sofiev, M. and Bergmann, K.-C. (2012). *Allergenic pollen: A review of the production, release, distribution and health impacts*. Springer Science & Business Media.

Stockdale, J. N. and Millwood, R. J. (2023). Transgene Bioconfinement: Don't Flow There. *Plants*, 12(5):1099.

Suanno, C., Aloisi, I., Fernández-González, D., and Del Duca, S. (2021). Monitoring techniques for pollen allergy risk assessment. *Environ. Res.*, 197:111109.

Techy, L., Schmale III, D. G., and Woolsey, C. A. (2010). Coordinated aerobiological sampling of a plant pathogen in the lower atmosphere using two autonomous unmanned aerial vehicles. *J. Field Robot.*, 27(3):335–343.

Tummon, F., Arboledas, L. A., Bonini, M., Guinot, B., Hicke, M., Jacob, C., Kendrovski, V., McCairns, W., Petermann, E., Peuch, V.-H., et al. (2021). The need for Pan-European automatic pollen and fungal spore monitoring: A stakeholder workshop position paper. *Clin. Transl. Allergy*, 11(3):e12015.

Vickers, D., Mahrt, L., and Belušić, D. (2008). Particle simulations of dispersion using observed meandering and turbulence. *Acta Geophys.*, 56:234–256.

Acknowledgments

This work is supported in part by the Biotechnology Risk Assessment Program, project award no. 2019-33522-29989, from the U.S. Department of Agriculture's National Institute of Food and Agriculture.

CRediT author contribution statement

Manu Nimmala: Methodology, Software, Formal analysis, Investigation, Data curation, Writing – original draft, Visualization.
Hope A. Gruszewski: Methodology, Investigation, Data curation, Writing – original draft, Visualization.
Regina Hanlon: Methodology, Investigation, Data curation, Visualization, Project administration.
Landon Bilyeu: Methodology, Investigation, Data curation, Writing – original draft.
Tyler Newton: Methodology, Investigation, Resources.
Jessica Stockdale: Methodology, Investigation, Resources.
Reginald J. Millwood: Methodology, Investigation, Resources, Writing – original draft, Project administration.
Charles N. Stewart: Conceptualization, Supervision, Funding acquisition.
Craig Powers: Methodology, Resources.
Shane D. Ross: Conceptualization, Investigation, Writing – review & editing, Supervision, Project administration, Funding acquisition.
Hosein Foroutan: Conceptualization, Investigation, Writing – review & editing, Supervision, Funding acquisition.
David G. Schmale III: Conceptualization, Methodology, Investigation, Writing – review & editing, Supervision, Project administration, Funding acquisition.

Competing interests

The authors declare no competing interests.

Declaration of generative AI and AI-assisted technologies in the writing process.

During the preparation of this work the authors used ChatGPT from Open AI in order to edit and improve original writing. After using this tool/service, the authors reviewed and edited the content as needed and take full responsibility for the content of the published article.